3D short fibre orientation for universal structures and geometries in material extrusion additive manufacturing

Jiongyi Yan, Emrah Demirci, Andrew Gleadall[*]

Wolfson School of Mechanical, Electrical and Manufacturing Engineering, Loughborough University, Loughborough LE11 3TU, UK

ARTICLE INFO

ABSTRACT

Fibre orientation critically affects properties in material extrusion additive manufacturing. This study developed new understanding of 3D short-fibre orientation in representative structures intended to capture most features of typical tool-paths. The parametric representative structures included straight paths, curved paths, corners, a range of intersection types, and the start/end of paths. Fibre orientation tensors were used to quantify 3D fibre alignment along the direction of printed filaments (F-alignment), lateral to the in-plane filament direction (F-lat alignment), and normal to the print-platform (Z-alignment). Overall, fibres were highly aligned along the filament direction in both straight paths and curved paths but less aligned at corners and intersections. However, recovery of fibre orientation was found after corners and intersections. To assess fibre orientation uniformity throughout the layer thickness, specimens were sectioned normal to the print platform in seven planes throughout the thickness of a single extruded filament. High fibre orientation (F-alignment) was found intra-filament, but it gradually decreased from upper section to bottom section. Interlayer region showed both high F-alignment and Z-alignment. In addition, extruded-filament width and height critically affected fibre orientation: increasing extrusion width and layer height led to decreased F-alignment. Case studies showed the results are translatable to more complicated structures and a different polymer material. This study provides new understanding of 3D fibre orientation in additive manufacturing and will allow more informed design, analysis and optimisation of short-fibre-reinforced structures to improve performance.

1. Introduction

Material extrusion additive manufacturing (MEAM) is an established process with increasing industrial demands [1,2]. As materials are innovated and modified, fibre reinforcements were introduced in MEAM to improve mechanical properties and functionality [3]. Discontinuous fibres, namely short fibres, are distributed within a polymer matrix to enhance strength and stiffness [4,5]. There are numerous studies attempting to improve mechanical properties with short fibre composites in MEAM [6–9]. Although it is challenging to achieve properties comparable to traditional composites (injection moulded, compression moulded, laminates), additively manufactured composites benefit from high flexibility in structural design [10]. With digital control of printing tools, complicated high-precision structures can be manufactured, which also allows the lay-up and controlled alignment of fibres. Hence, short fibre orientation is controllable and potentially predictable in MEAM. Fibre orientation plays an important role in the process-structure-property correlation and directly affects final properties [11], as higher fibre orientation leads to higher strength and modulus [12]. However, fibre orientation also affects anisotropy, as fibres strengthen the longitudinal direction but weaken the transverse direction [13]. It is important to study fibre orientation to understand and improve properties in MEAM. Fibre orientation could be affected by processing conditions (temperature) [14], melt viscosity [15], flow properties [16], nozzle geometries (shear) [17], die swell [18], and print-structure geometry [14].

Short fibre orientation has been studied via experiment characterisation and computational simulation [2]. Short fibres were found to be highly oriented in the filament direction (F direction, frequently referred as the longitudinal direction). Ref. [14] studied fibre orientation distribution with a 2D planar fibre orientation model and reported highly oriented short fibres in the F direction. Extrusion width was found to be critically important and fibre orientation decreased with increasing extrusion width. Ref. [19] quantified 3D short fibre orientation with orientation tensors [20] and reported high F-direction fibre alignment, low in-plane transverse direction fibre alignment, and low Z-direction fibre alignment. Ref. [21] reported high orientation along the print

* Corresponding author.
  E-mail address: A.Gleadall@lboro.ac.uk (A. Gleadall).

Nomenclature

a_{11}	Fibre alignment in the filament longitudinal direction (F-alignment).
a_{22}	Fibre alignment in the in-plane filament lateral direction (F-lat alignment).
a_{33}	Fibre alignment in the out-of-plane Z building direction (Z-alignment).
ABS-CF	Carbon fibre reinforced acrylonitrile-butadiene-styrene.
F direction	Along the direction of extruded filaments (printing direction).
H	Layer height of printed filaments.
MEAM	Material extrusion additive manufacturing.
PLA-CF	Carbon fibre reinforced polylactic acid.
W	Nominal extrusion width of printed filaments (set in GCode).
Z direction	Direction normal to the build platform (normal to filament interlayer interface).

paths and low orientation at filament intersections via computed tomography (CT). Ref. [22] reported greater fibre orientation in the nozzle (before extrusion) compared to in printed filaments. CT is capable of 3D modelling fibres, but it is time-consuming, which limits practical application for most industrial applications. Hence, the two studies that use CT scans to characterise fibre orientation in MEAM specimens only considered a single specimen type. Stereological measurement of elliptical fibre cross-sections [20] allows cost-effective characterisation by microscopy and image processing in a timely manner, which enables a wide range of parametric specimens to be considered in the present study. Also, X-ray CT scanning relies on material densities, where two materials with similar densities may be indistinguishable, as was experienced by the authors of this study in preliminary research. Aside from these studies, fibre orientation was primarily characterised qualitatively in the literature, including microscopy at fracture surface [23–26] and sectioned printed filaments [27]. Computational simulation was implemented to study fibre orientation using a planar deposition flow model [28], Newtonian fluid models [29], coupled flow-fibre finite element method [30], and a particle element approach [31]. Ref. [28, 29] reported high orientation inside the nozzle and decreased orientation after exiting the nozzle due to die swell. Non-uniform fibre orientation in the in-plane transverse direction was identified [28]. However, variation of fibre orientation in the Z direction was never studied. The study of spatial fibre orientation distribution is of particular interest because filament interlayer is intrinsically different from the internal region of an extruded filament and fibre orientation may affect the interlayer anisotropy [32]. To understand fibre's role at the filament interlayer and interlayer properties, a study of fibre orientation distribution throughout the layer thickness is needed.

There is currently a lack of understanding about how fibres are oriented in different geometric paths since previous research mostly considered straight print paths. Ref. [33] quantified fibre orientation in straight paths and used homogenised properties to study deformation at circular corners. The vast majority of 3D printed parts utilise complicated paths with curved and straight regions, corners, intersections, and other features. A thorough study of fibre orientation in universal structures and geometries is needed to understand how fibre orientation is affected by structural design and toolpath design, and to identify major factors affecting fibre orientation. By studying fibre orientation in-depth, high-performance printing and products may be achieved [34].

This is the first study to map out fibre orientation for universal structures and geometries and develop new understanding of short fibre orientation in 3D printing. The universal geometries include straight paths, curved paths, corners, a range of different types of filament intersections, and printing start and end points. This presents a comprehensive picture of fibre orientation relevant to both simple and complex print paths. Furthermore, the effects of extrusion width and layer height on fibre orientation were investigated, as well as variation of fibre orientation throughout the thickness of a layer, including assessment of the intra-filament and interlayer area regions. Case studies showed how findings are relevant to complicated 3D print structures and translate to other materials.

2. Experimental methodology

2.1. Materials

CARBONX™ carbon-fibre-reinforced polylactic acid (PLA-CF) and carbon-fibre-reinforced acrylonitrile-butadiene-styrene (ABS-CF) with 1.75-mm filament diameter and 15 wt% short carbon fibre [27] were used (3DXMAX™, 3DXTECH®, USA). A micrograph of the cross-section of the feedstock PLA-CF filament is presented in Supplementary Data. PLA-CF was used throughout the main study. ABS-CF was used as an alternative material in a case study to evaluate result translatability in Section 3.6.3.

2.2. Additive manufacturing and specimen preparation

A Raise3D® Pro2 3D printer with a hardened steel nozzle (diameter 0.4 mm) was used for additive manufacturing. To allow thorough understanding of fibre orientation for common print-paths, multi-layer single-filament specimens with various paths and geometries were developed. This includes straight paths, curved paths, corners, a range of intersections, and printing start/end points, as shown in Fig. 1. Full-Control GCode Designer [35] was used to generate manufacturing GCode since it allows explicit control of print paths through parametric design. All specimens had a reference extrusion width (W) of 0.6 mm, controlled by the E value in GCode that dictates material flow, and layer height (H) of 0.2 mm, which was controlled by the distance between the nozzle and the print platform or the material deposited as the previous layer. All specimens consisted of ten layers.

Straight paths and a range of corner geometries were evaluated with a single multi-purpose specimen (Fig. 1(a)). Straight path sections were used to study the effects of extrusion width and height (equivalent to layer thickness) on fibre orientation. W was varied from 0.4 and 0.8 mm and H was varied from 0.1 to 0.3 mm, as shown in Table 1. Straight sections were also used to assess how fibre orientation varied throughout the thickness of a layer, including the intra-filament and interlayer-bond regions, by sectioning at seven planes parallel to the print platform (Z direction) (Fig. 1(e)). Corner-angles of 30°, 60°, 90°, 120°, and 150° were used to study fibre orientation at corners.

To study fibre orientation in curved paths, circular and sinusoidal constructs were printed (Fig. 1(b)). The circular construct had a diameter of 4 mm. The sinusoidal print-paths were designed with sinusoidal functions of $y = \sin(x \bullet 2\pi)$ and $y = 2\sin(x \bullet 2\pi)$ for different amplitudes.

To study fibre orientation at filament intersections, several junctions were considered: a cross junction, 'T' junction, bouncing junction, and circular tangential junction (Fig. 1(c)). For cross, T, and bouncing junctions, a straight line was printed first, before the second filament was printed perpendicular to the first line. For the bouncing junction, the second filament approached at $+45°$ relative to the F-direction of the first filament and departed at $-45°$ after contacting it. The fibre orientation before the junction, at the junction, and after the junction was studied for both lines in each case, which is described in Section 2.3. For T, bouncing, and circular-tangential junctions, the print paths of the two lines perfectly coincided at the point of the junction.

To study fibre orientation at the start point and end point of printed lines (Fig. 1(d)), a specimen was designed and consisted of a square-shaped print path for which only one of the sides of the square was
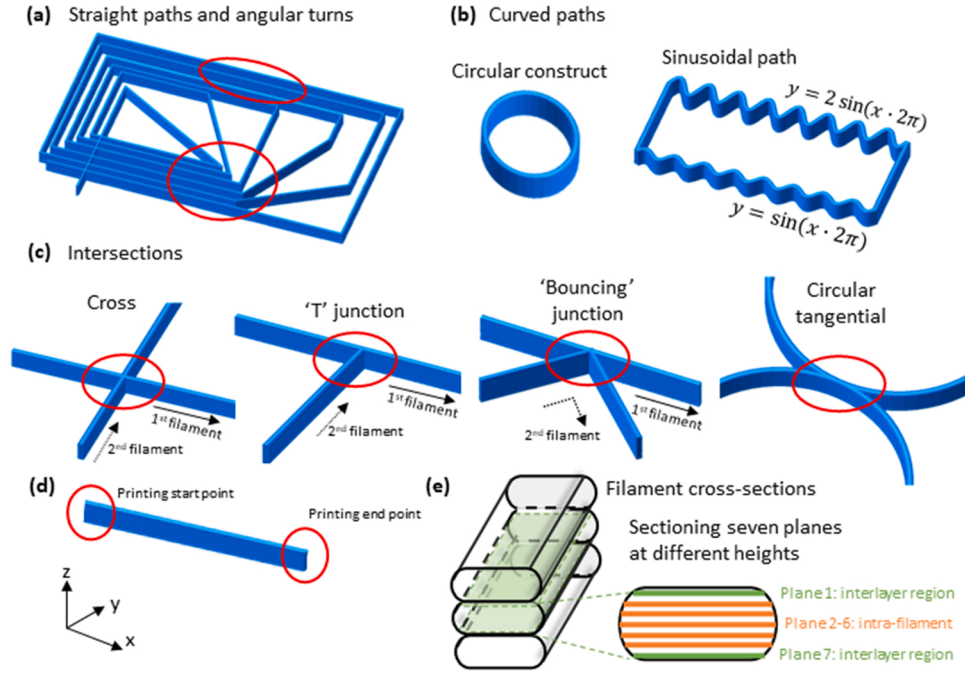
Fig. 1. Structure design of 3D printed single-filament-wide multi-layer specimens. (a) Straight paths and corners (0/30/60/90/120/150°). (b) Curved circular and sinusoidal paths. (c) Path intersections including cross junction, 'T' junction, 'bouncing' junction, and circular tangential junction. (d) Printing start and end points. (e) Straight-path specimen sectioning through a filament seven times in the Z direction.

Table 1
Printing conditions of specimens. The reference-specimen values (bold font) are used for all specimens except those that specifically vary parameters about the reference values (italic-font).

Parameters	Set values
Set extrusion width W (mm)	*0.4*, **0.6**, *0.8*
Layer height H (mm)	*0.1*, **0.2**, *0.3*
Nozzle temperature (°C)	220
Bed temperature (°C)	60
Printing speed (mm.min⁻¹)	1000
Nozzle travel speed (mm.min⁻¹)	6000
Cooling conditions	Cooling fan on maximum, cooled in the air

printed. For the other three sides of the square, the nozzle executed non-extruding travel movements to return to the same start point, one layer higher. The printed line had a length of 40 mm.

All specimens were mounted in epoxy resin and cured in the air. The sectioning method was reported in [14], where sections were prepared by an auto-polisher. It involved grinding with 1200 grit sandpaper (300 rpm and 20 N) then polishing with 3 μm polycrystalline diamond suspension (MetaDi™Supreme) (150 rpm and 20 N) and 0.05 μm alumina suspension (BUEHLER MasterPrep™) (150 rpm and 15 N). To study spatial fibre orientation across filaments in the Z direction, straight-path specimens were sectioned with controlled repeated grinding (20 s) and polishing (1 min) within one single extruded filament layer from the top interlayer area to the bottom interlayer area. Seven section-planes were produced with five considered as intra-filament and two considered to be at the interlayer region: the top and bottom planes closest to interlayer bonds. Other samples were always ground and polished around the middle of printed filaments to ensure comparable filament geometry.

2.3. Microscopy and image post-processing

A Zeiss Primotech optical microscope with a 5× magnification lens was used for observation of fibres. As samples were ground and polished,

fibre cross-sections were exposed as ellipses. Stereological measurement [20] of elliptical fibre cross-sections enables the characterisation of out-of-plane angle in Z axis (Euler angle, θ) and in-plane angle (the angle of the ellipse oriented relative to the printing direction, ϕ) of a fibre, as shown in Fig. 2(a) and (b). By averaging all fibres on a sectioned plane statistically, the fibre orientation tensor, which quantifies 3D fibre orientation, is given in Eq. (1),

$$A_{ij} = \begin{bmatrix} a_{11} & a_{12} & a_{13} \\ a_{21} & a_{22} & a_{23} \\ a_{31} & a_{32} & a_{33} \end{bmatrix}$$
$$= \begin{bmatrix} \sin^2\theta\cos^2\theta & \sin^2\theta\cos\phi\sin\phi & \sin\theta\cos\theta\cos\phi \\ \sin^2\theta\cos\phi\sin\phi & \sin^2\theta\cos^2\phi & \sin\theta\cos\theta\sin\phi \\ \sin\theta\cos\theta\cos\phi & \sin\theta\cos\theta\sin\phi & \cos^2\theta \end{bmatrix} \quad (1)$$

a_{11} is the fibre alignment in the printing direction (F direction). a_{22} is the lateral fibre alignment in the width direction of printed filaments (transverse to the F direction). a_{33} is the out-of-plane fibre alignment in the Z direction (normal to the interlayer bond). A value approaching 1 for any of these terms indicates that all fibres are perfectly aligned in the given direction. A value approaching 0 indicates all fibres are oriented normal to the given direction. However, fibres perpendicular to the sectioning surface are more likely to be observed than fibres parallel to the sectioning plane. To correct the biased sampling, a weighting factor is added to render fibres parallel to the observation plane with more weight, according to Eq. (2).

$$w_i = \frac{1}{\cos\theta_i} \quad (2)$$

Thus, the modified fibre orientation tensor is given in Eq. (3),

$$A'_{ij} = \frac{\sum_k w_k A_{ij}}{\sum_k w_k} = \frac{\sum_k w_k p_i^k p_j^k}{\sum_k w_k} \quad (3)$$

In this work, a_{11} was always measured F-direction fibre orientation (along printing direction), and a_{22} was always measured the in-plane transverse direction (F-lateral-direction). The straight path specimens always had the main printing direction as the F-direction, as shown in Fig. 2(c). For corners, a_{11} was measured in different directions before
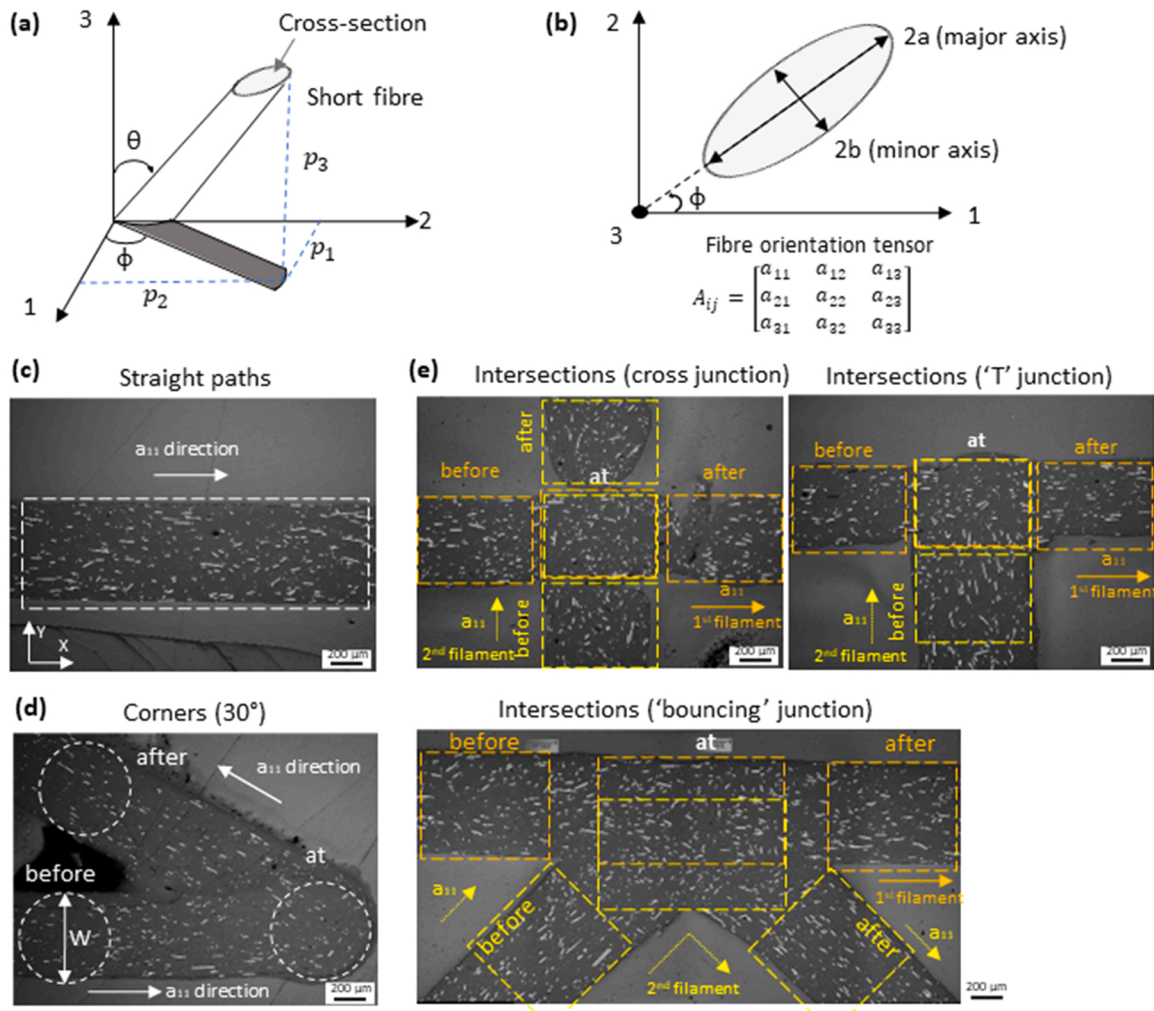
Fig. 2. Measurement of fibre orientation. (a) stereological measurement of elliptical fibre cross-sections (b) characterisation of ellipses for fibre orientation tensors. Fibre orientation measurement for (c) straight paths, (d) before, at and after corners, and (e) before, at and after intersections for the first- and second-printed filaments.

and after corners depending on the turning angle. For example, for 30° corner, the F-direction after the corner was 30° relative to the F-direction before the corner, as shown in Fig. 2(d). A circular area of interest with the diameter of W was used to measure fibre orientation before, at, and after corners. For intersection specimens, fibre orientation for the first and second filaments were measured separately in their own directions. For the cross and 'T' junctions, the F-direction was constant (horizontal and transverse). For the 'bouncing' junction, the second filament had a F-direction 45° relative to the first line before the junction and − 45° after the junctions, as shown in Fig. 2(e). For statistical significance, areas of interest always had more than 200 fibres for fibre orientation measurement.

3. Results and discussion

This section first considers straight paths to evaluate spatial variation of fibre orientation throughout an extruded filament and for different extrusion widths and heights. Then the effects of corners, curved paths, intersections, and printing start/end points on fibre orientation are analysed. Finally, three case studies of complicated geometric structures and alternative materials are used to demonstrate transferability and applicability of results.

3.1. Fibre orientation in straight paths

3.1.1. Fibre orientation at Intra-filament and interlayer region

Printed filaments had non-uniform cross-sections through their thickness, as is expected for layer-by-layer deposition. Filament width continuously varied across layers in the Z direction. It was wider in the filament centre and narrower at top/bottom interlayer-bond regions. Seven sectioned planes through the thickness of one printed filament layer are shown in Fig. 3(a and b). Sectioned planes 2–6 had measured filament-width (598 ± 4 μm) similar to set extrusion width 600 μm, because these planes were close to the filament centre. The measured width decreased by 10.4% to 545 ± 9 μm for planes 1 and 7, indicating filament interlayer regions near to the upper and lower interlayer bonds.

Fibre orientation at all section planes showed a consistent trend that F-alignment a_{11} (0.751 ± 0.120) was always the highest compared to F-lateral alignment a_{22} (0.091 ± 0.083) and Z-alignment a_{33} (0.164 ± 0.042), as shown in Fig. 3(c). Fibres were always highly aligned in the F direction in the extruded filaments, at both intra-filament and interlayer regions, even though the width change at different positions. However, there were variations in fibre orientation between the sectioned planes. From plane 2 to plane 6, F-alignment a_{11} continuously decreased by 28.6%, while F-lateral alignment a_{22} and Z-alignment a_{33} increased by 341% and 59.6% respectively. This shows that fibres were more randomly oriented in the bottom intra-filament section, which was
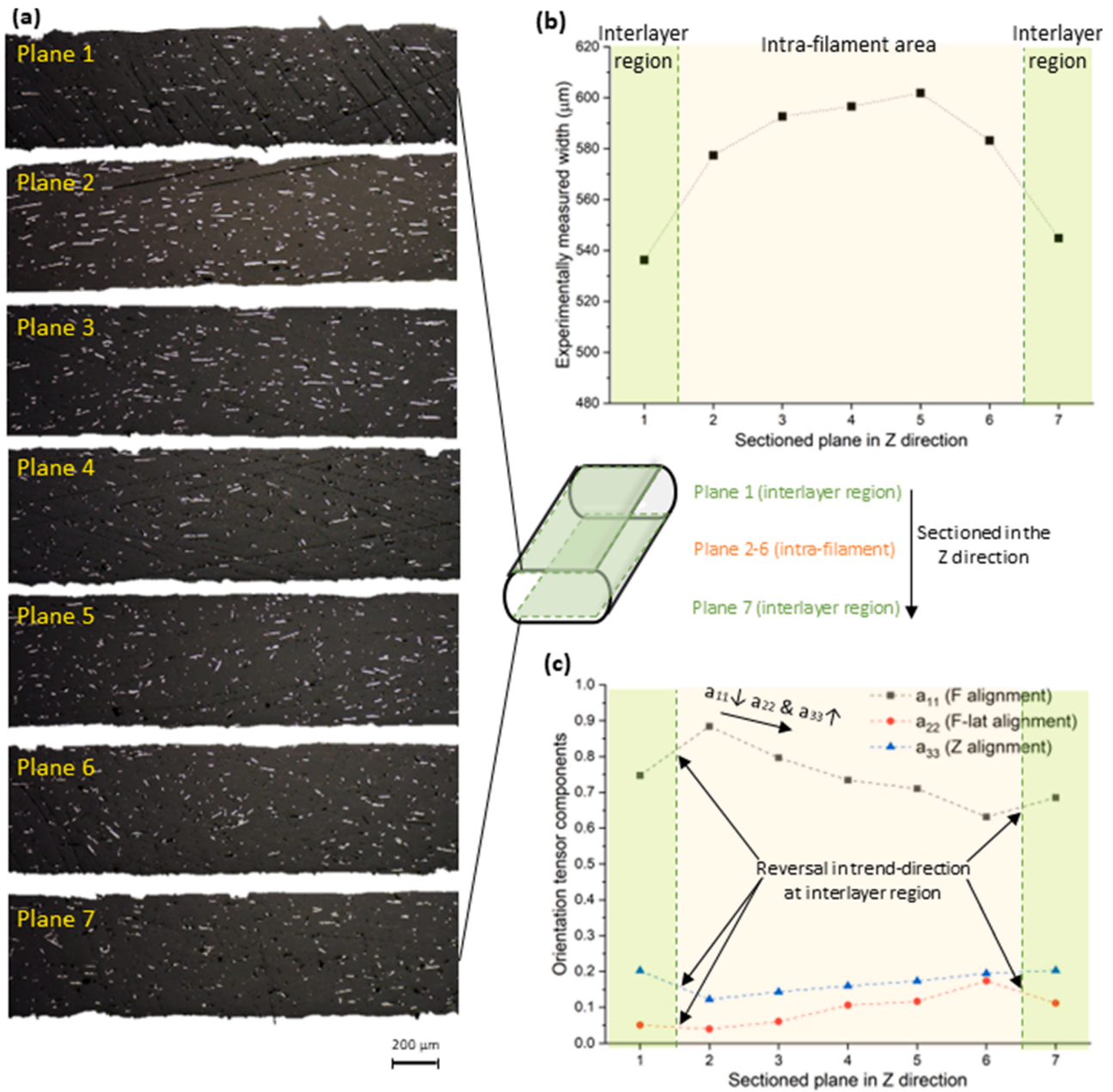
Fig. 3. Fibre orientation at intra-filament and interlayer regions at the sectioned planes in one printed filament in the Z direction. (a) Micrographs of the seven sectioned planes. (b) Measured filament width of the sectioned planes. (c) Fibre orientation across the filament. Intra-filament regions (Section 2 to 6) and interlayer regions (Section 1 and 7) are shaded yellow and green, respectively, in (b) and (c).

likely caused by shear at nozzle exit, where the top-section melt is subject to greater shear at the nozzle exit due to a sharp turn than the bottom section. Due to cyclic layer-wise manufacturing, it is logical for Z-direction trends to be reversed across the interlayer region since orientation trends will repeat layer-by-layer. Hence, fibre orientation rapidly changes across the interlayer region. Overall, the interlayer region (planes 1 and 7) was found to have high Z-alignment a_{33} (0.202), which was 42% greater than the average a_{33} plane-2 to plane-6. This suggests more fibres were oriented out-of-plane in the Z direction at filament interlayer, potentially due to more turbulent melt-flow and diffusion at the interface between layers during coalescence.

Overall, fibres were highly aligned in the F direction throughout the intra-filament and interlayer areas in the extruded filament. Spatially non-uniform fibre orientation was found, where fibres were more aligned in the upper section than the bottom section intra-filament.

Compared to intra-filament, the interlayer region had higher Z-alignment.

3.1.2. Filament geometry effects on fibre orientation

Width (W) and height (H) of the extruded filament were varied to study the effects of filament geometry on 3D fibre orientation. As W increased from 0.4 mm to 0.8 mm, F-direction fibre alignment a_{11} decreased by 32.7% from 0.831 to 0.558, as shown in Fig. 4(b). Meanwhile, a_{22} and a_{33} increased by 530% and 75.1%, respectively. At lower W, fibres were constrained spatially to be more oriented in the F direction. However, greater W means less spatial constraint and longer cooling, which may induce more lateral flow and out-of-plane flow of fibres. The result agrees the extrusion width effects on planar fibre orientation [14]. As H increased, a_{11} decreased by 16.5% from 0.833 to 0.696, while a_{22} and a_{33} increased by 249% and 45.5% respectively
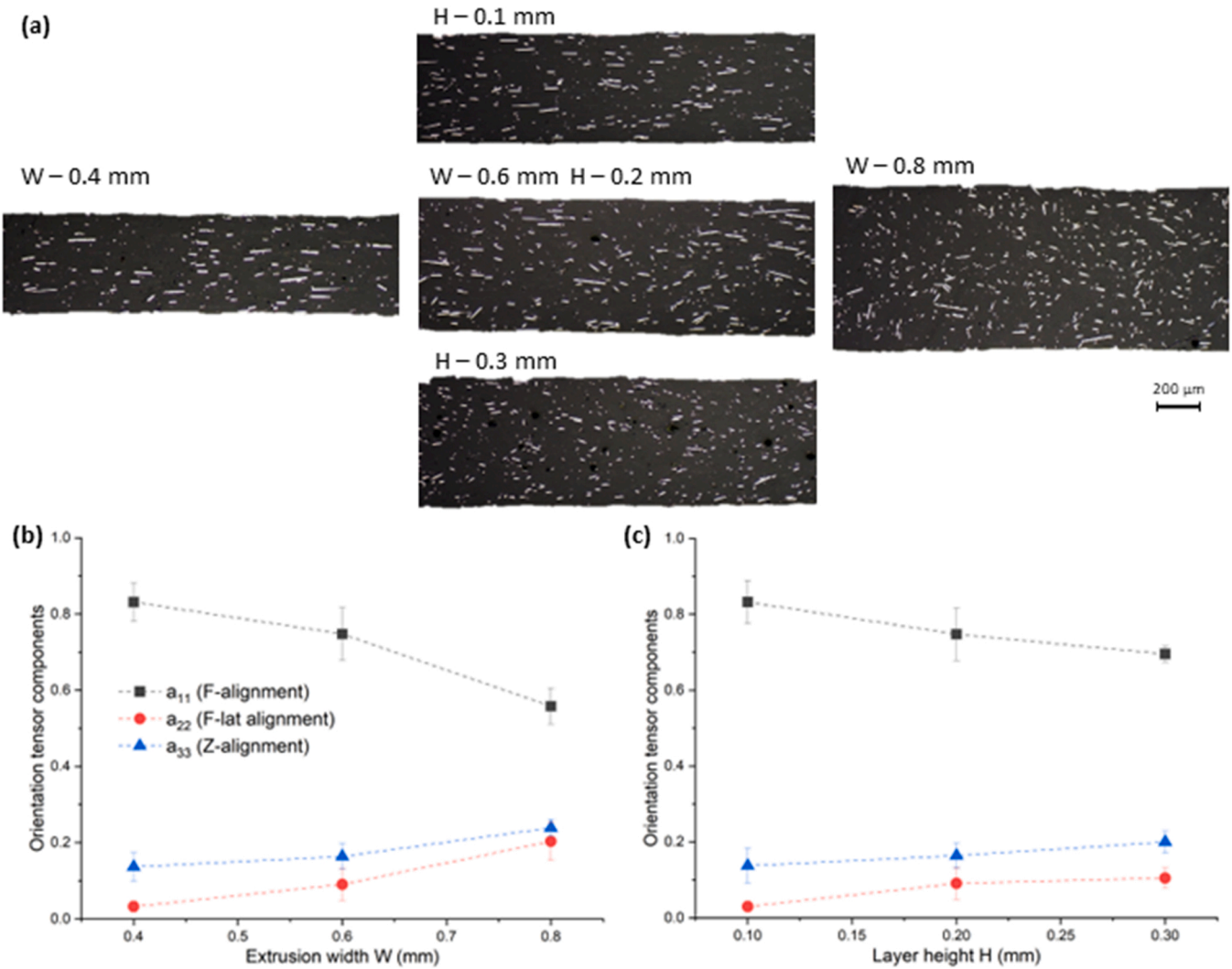
Fig. 4. The effects of filament geometry on fibre orientation. (a) Micrographs of printed filaments with different W (0.4/0.6/0.8 mm) and H (0.1/0.2/0.3 mm). Fibre orientation for a range of (b) extrusion widths and (c) layer heights. Longitudinal fibre orientation decreased with increasing W and H. Error bars stand for standard deviation of fibre orientation throughout the specimen thickness at seven sectioned planes.

(Fig. 4(c)). This shows that fibres were more aligned longitudinally for lower layer heights, likely due to the similar geometric constraints as discussed for lower widths. Lower heights may also induce greater shear that imposes high fibre orientation [36], whereas higher H offered fibres more freedom to flow vertically with and longer cooling, so more fibres were oriented out-of-plane. In addition, error bars in Fig. 4 represents fibre orientation variation throughout a layer thickness sectioned at seven planes. Compared to a_{11} variation caused by W ($\sim$49%) and H ($\sim$20%), spatial variation only caused $< 17\%$ a_{11} variation, suggesting the filament geometry is more influential than the spatial distribution.

Both W and H showed the same trends, where lower W and H caused higher F-direction fibre orientation. The Z-direction and lateral fibre orientations both increased with increasing W and H. This reveals the consistent and critical influence of filament geometry on fibre orientation for structure-property relationships in MEAM. Since fibre orientation is important for many properties including mechanical, thermal, and electrical properties, the geometry-dependent fibre orientation should be considered. Although it is not possible to study all properties of interest in a single study, tensile testing specimens are tested here to evaluate the link between fibre orientation and elastic modulus. PLA-CF was 3D printed into single-filament-wide specimens with varied W (0.4/0.6/0.8 mm) and H (0.2/0.25/0.3 mm). Details of procedures for additive manufacturing, specimen preparation, and tensile testing are

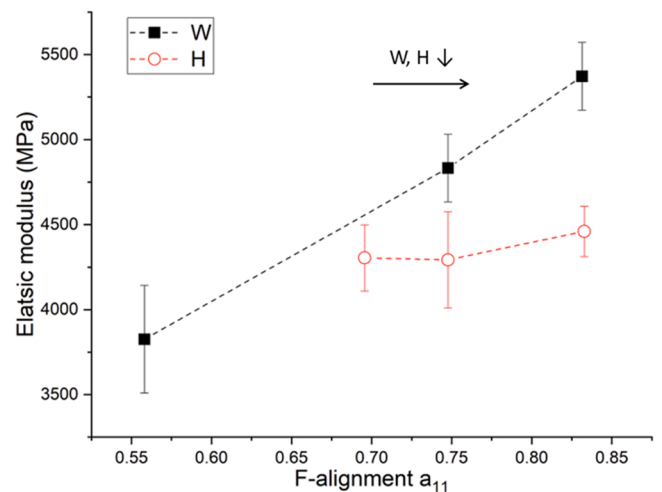included in [37]. Fig. 5 shows that elastic modulus increased with

Fig. 5. Elastic modulus increased with fibre F-alignment with decreasing extrusion width (W) and height (H). Error bars represent standard deviation of five replicas.

decreasing W and H due to lower fibre orientation, which agrees the literature [14]. There is a statistically significant link between fibre orientation and elastic modulus for specimens with varying width ($p<0.05$) but the trend for varying height is not significant even though there is a slight trend. There are apparently other factors affecting the stiffness with varying height, potentially linked to lower layer heights increasing shear stress in the melt flow and increasing the number of layer interfaces, which may introduce defects or porosity [16]. Importantly, the results for fibre orientation found that it was more influenced by variation of width than height, and this was also the case for the influence on elastic modulus. Therefore, it is recommended that extrusion width is a more suitable parameter for varying fibre orientation than layer height. Mechanical testing of more complex geometries in subsequent results sections (intersections, corners, and curves) is not in scope for this study because such tests would require new testing methods. Their characterisation is an interesting area of future research, along with the evaluation of other mechanical properties including fatigue and flexural and non-mechanical properties including thermal and electrical. With regards to fibres' inherent anisotropy, a balance of structural and composite anisotropy should be considered. For example, low W and H may have lower interlayer strength due to more frequent inter-filament and interlayer geometry defects. Hence, optimisation of filament geometry is needed to get desirable properties and anisotropy.

Another concern is the balance of cost and quality of 3D printed fibre composites in a practical setting. Despite high fibre orientation, using lower W and H may increase the printing time and energy cost. The strong dependency of fibre orientation on filament geometry highlights that W and H should be carefully designed in future research of 3D printed short-fibre-composites. For big area additive manufacturing incorporated with post-extrusion processing (tamper, roller, etc.), surface treatment may change printed filament geometry and therefore fibre orientation. Future research could further analyse fibre orientation with various forms of hybrid manufacturing.

3.2. Fibre orientation at corners

Fibre orientation at corners with angles of 30°, 60°, 90°, 120°, and 150° was studied. All specimens showed great F-direction alignment a_{11} (0.746) before corners, as shown in Fig. 6(b). All specimens showed reduced F-alignment of fibres at corners. For 30° and 150°, a_{11} decreased by 14.5% and 24.1% respectively at corners, whereas greater reductions in a_{11} were found for 60°, 90°, and 120° (44.3% ± 3%). A turning angle more deviated from the original F-direction would result in lower orientation at corners, as a_{11} measured the F-direction before corners. Thus, the decrease in a_{11} was smaller for 30° and 150° than 60°, 90°, and 120°. All specimens showed increased a_{11} after corners, except
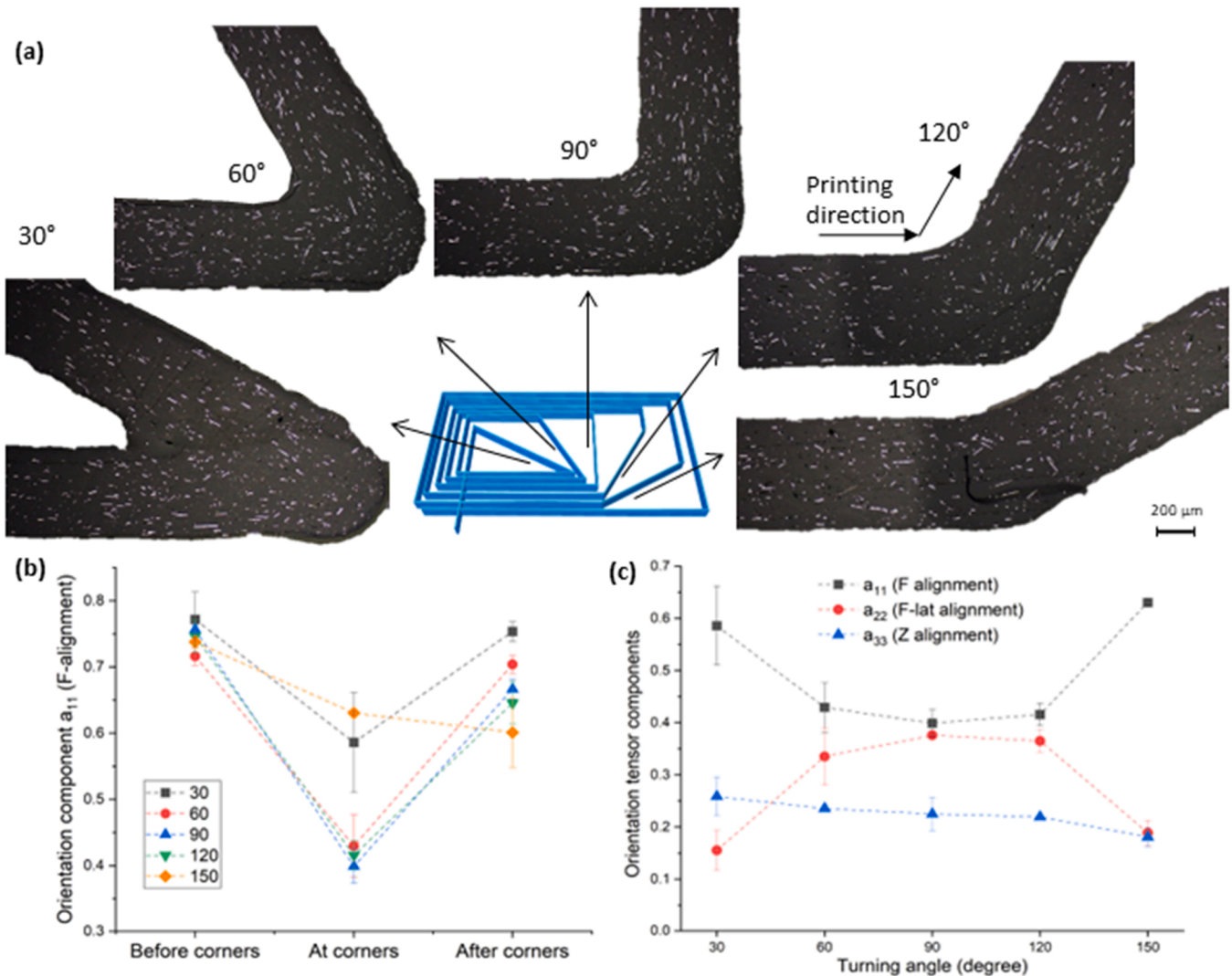

Fig. 6. Fibre orientation for corner angles of 30/60/90/120/150°. (a) Micrographs of specimens (b) Longitudinal fibre orientation measured before corners, at corners, and after corners. (c) Fibre orientation components at corners for all angles. Error bars give the maximum and minimum values for three specimens.

150°. The a_{11} increased to 0.753 for 30°, followed by 60° (0.704), 90° (0.667), and 120° (0.646), suggesting high fibre orientation in the new F-directions after corners. Their a_{11} after corners for all angles was similar to before corners (only lower by 1.7%–13.4%). The measurement areas after corners were close to the corner point (<1000 μm), which shows the rapid recovery of fibre orientation after turns. The 150° specimen showed decreased a_{11} after turns (lower by 18.5% than before turn), which might be related to delayed turbulence and require further investigation. Overall, fibre orientation decreased at turning corners, and it recovered rapidly after turns.

There are consistent trends of 3D fibre orientation at corners, as can be seen in in Fig. 6(c). a_{11} and a_{22} showed opposite trends with angles. As the turn angle increased from 30° to 90°, a_{11} decreased by 32% from 0.586 to 0.399, while a_{22} increased by 143% from 0.155 to 0.376. As the angle increased from 90° to 150°, a_{11} increased by 58% to 0.630, while a_{22} decreased by 50% to 0.189. The a_{22} peaked at the 90° corner, where a_{11} was the lowest, suggesting that fibres were more likely to be oriented

in the lateral direction relative to the original F-direction. This is logical because the 90° turn was transverse to the F-direction and encouraged fibre lateral-alignment.

As for out-of-plane Z-alignment of fibres, a_{33} continuously decreased from 0.259 at 30° to 0.181 at 150°. For corners lower than 90°, the nozzle printed back over material that was already deposited. The overlap area could cause over-extrusion, inter-filament diffusion, and disruption to material flow directions, leading to more out-of-plane fibre orientation. It is hypothesised that when the nozzle moved over the newly deposited material in the nearly opposite direction, the deposited material would have been disturbed, naturally leading to a reduction in shear-induced fibre alignment. Also, the 30° corner showed over-extrusion on both inner and outer radii, which may have led to greater Z orientation of fibres as discussed in relation to in Fig. 4(b) for wider extruded filaments. The over-extrusion for sharp corners agrees the literature [38].

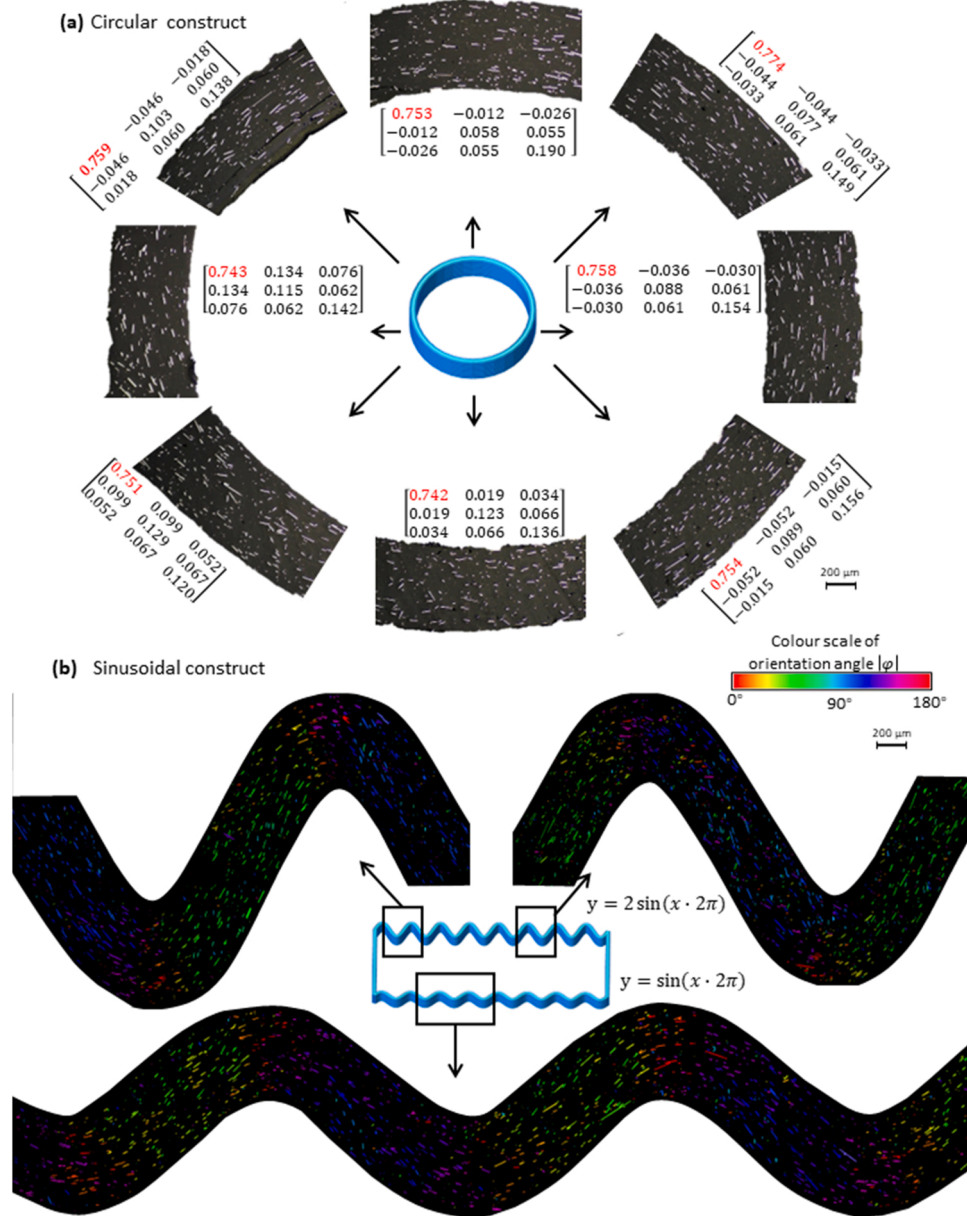Overall, low fibre orientation at corners was found, where it was the

Fig. 7. 3D Fibre orientation in curved paths (a) circular path sampled at eight points around the circle and the measured orientation tensor. (b) sinusoidal path segments with different sinusoidal amplitudes. Fibres were coloured according to their in-plane orientation relative to the sinusoidal axis, which clearly shows that fibres were highly oriented in the instantaneous printing direction.

lowest at 90° and increased towards 0° and 180°. There was a strong correlation of fibre Z-alignment decreasing as the corner angle decreased. These findings will help understand fibre-orientation in with complicated print-paths and infill patterns, which often include frequent corners with various corner angles. Sharp angles may induce more fibre Z-alignment and impair in-plane properties. Corners should be carefully designed not only for aesthetics or cost efficiency but also practical consideration of holistic properties to avoid mechanical weakness.

3.3. Fibre orientation for curved paths

In curved printing paths, characterisation of fibre orientation was challenging because the F-direction, and therefore a_{11}, was constantly changing. Therefore, the path was sampled at eight points around the circle (0°, ± 45°, ± 90°, ± 135°, 180°), as shown in Fig. 7(a). Each segments used a relatively narrow arc angle (36° ± 3°) and low curvature (0.003 ± 0.0007) to ensure the F-direction was relatively unidirectional throughout the entire sample. Overall, fibres were highly oriented along the filaments for all eight samples, with high a_{11}, low a_{22} and low a_{33}, similar to the reference specimen for straight lines in Fig. 4 (b) and agrees with literature [33], suggesting the straight-line results could translate to curved paths. In the sinusoidal paths, fibres were colour-coded on a spectrum based on their in-plane orientation angles relative to the sinusoidal axis, as shown in Fig. 7(b). It can be seen from the colour map that fibres were clearly oriented along the filaments.

Fibres were mostly oriented around 0° in the peak amplitude sections and at approximately 30–60° and 120–150° for the straight sections, depending on the amplitude of the sinewave, which logically directly affected the in-plane angles of straight sections. The clear colour-gradient around peak-amplitude sections indicates that fibre orientation smoothly transitioned around the curved sections of paths.

3.4. Fibre orientation at intersections

Studying fibre orientation at intersections allows better understanding of how two extrudates interact. For the cross junction, the first filament and second filament had distinct trends of fibre orientation before, at, and after the junction, as shown in Fig. 8(a). From before the junction to after the junction, the first filament had decreased a_{11} (by 23.7%) and increased a_{22} (by 16.4%) and a_{33} (by 73.1%). For the second filament, a_{11} first decreased by 61.4% and then increased by 80.3%, whilst a_{22} increased by 129% to at the junction and then decreased by 35.5%. Meanwhile, a_{33} increased by 17.0% from before to after the junction. The first filament had higher fibre orientation than the second filament because the first filament was printed in a steady state, whereas fibres in the second filament were subject to interference in the transverse direction. The fibre orientation decreased at the junction for both filaments, which suggests intersecting filaments printed in different directions affected and interfered each other. Noticeably, filament geometry was affected by the intersection. The second filament showed a
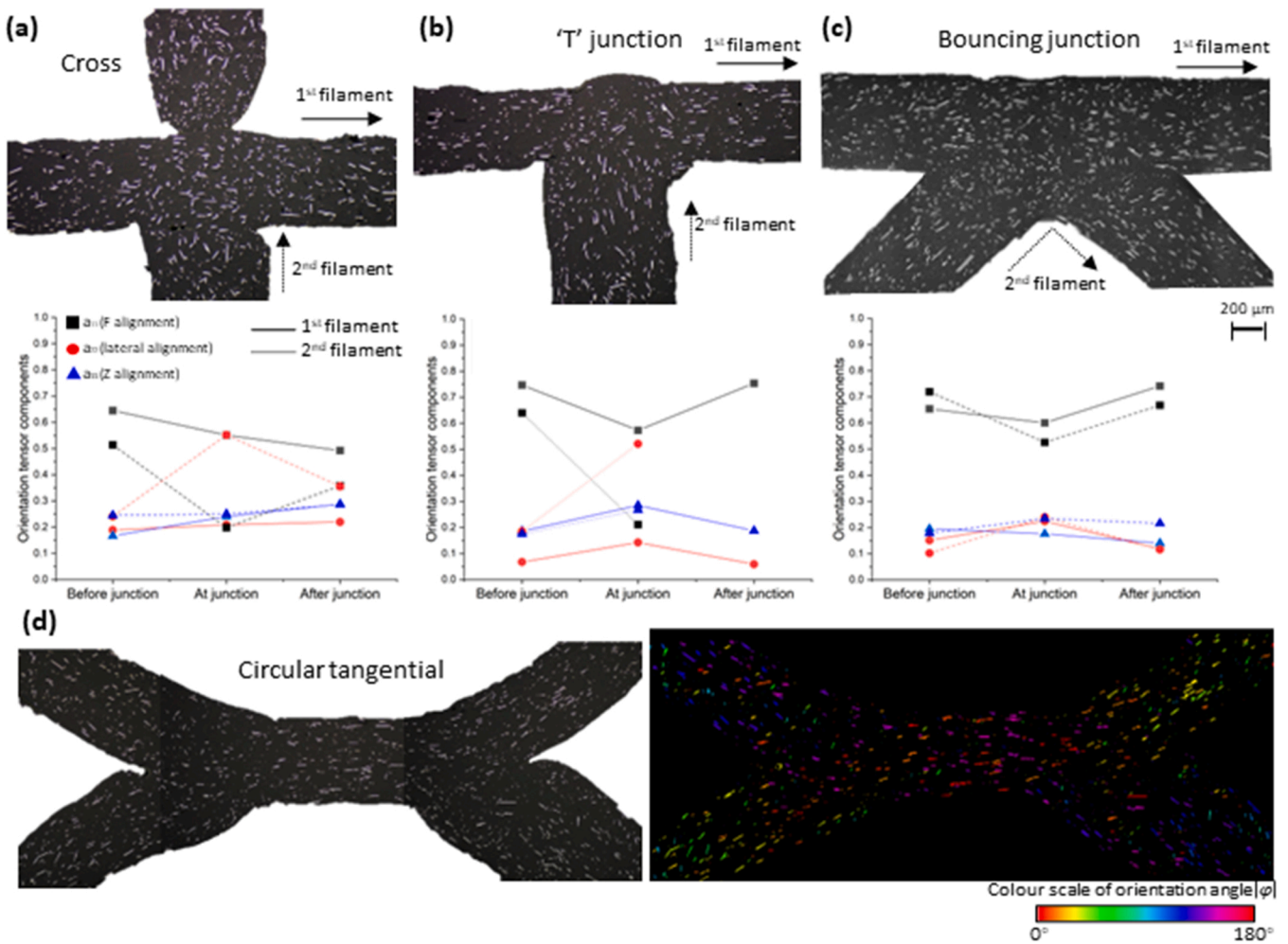

Fig. 8. Fibre orientation at filament intersections. Micrographs and fibre orientation tensor components of intersecting filaments for (a) cross junction, (b) 'T' junction, and (c) 'bouncing' junction. (d) Micrograph and colour map for fibre orientation of circular tangential intersection. Fibres were coloured according to their in-plane orientation relative to the medial axis of the intersecting region, which clearly shows that fibres were highly oriented in the instantaneous printing direction.

slightly decreased width when approaching the junction and exiting the junction (~50% of the W). After that, the width gradually increased to the designated W as it was printed away from the junction. This phenomenon was reproducible with different W and H, probably due to filament interactions with the nozzle. As the nozzle moved across a deposited filament and still attempted to extrude material, the nozzle exit was obstructed and flow could not be immediately re-established after passing the obstruction, resulting in under-extrusion immediately after the intersection. Finally, fibre alignment was rapidly recovered for the second filament, probably due to greater shear and under-extrusion after the turbulence, but the first filament had no opportunity to recover, as it was already printed and affected by the second filament with thermal diffusion.

For the 'T' junction, fibre orientation decreased at the junction, as shown in Fig. 8(b). The a_{11} decreased by 23.3% at the junction, while a_{22} and a_{33} increased by 111% and 53.3% respectively. The second filament showed decreased a_{11} (by 67.0%), increased a_{22} (by 182%), and increased a_{33} (by 52.9%). This showed low fibre orientation at the junction due to the mutual interference. Interestingly, a_{11} of the first filament recovered by 31.5% after the junction, suggesting limited effects of the second filament.

For the bouncing junction, fibres were also lowly oriented at the junction, as shown in Fig. 8(c). a_{11} decreased by 8.6% and 26.9% at the junction for the first and second filaments respectively, while it increased by 23.5% and 27.0% respectively after the junction. The second filament made a turn at $\pm 45°$ deviated from the intersection point, resulting in low fibre orientation. The a_{22} increased by 48.2% and 136% for both filaments respectively, indicating more inter-diffusion. Interestingly a_{33} of the second filament increased by 31.2%. This suggests the increased out-of-plane fibre orientation of the second filament at junction, which may be caused by the over-extrusion at the junction corner.

The circular tangential intersection showed high fibre orientation, as shown in the colour map in Fig. 8(d). In the contact area, most fibres were aligned in 0° in the F direction. This indicates that filament interference could be diminished by adjusting how two filaments intersect and their printing directions. Overall, low fibre orientation was found at junctions. Filament intersections had adverse effects on fibre orientation depending on the second filament printing direction. Additionally, disruptive under-extrusion and orientation recovery of the second filament after the junctions were found. The study of intersections is important for design and mechanics of infill patterns of 3D printed parts. Lattice-like infill patterns, consisting of separate struts, are the most common printing strategy in 3D printing for low density, low cost, and material saving compared to solid parts. In practice, infill lattices with various geometries are used, like grid, triangle, hexagon, concentric, and gyroid. For most infill lattices, the printed filaments

intersect, where the filament geometry and fibre orientation could be affected. The findings here allow fibre orientation at intersections to be quantified and will hopefully guide the infill pattern design based on desired fibre orientation.

3.5. Fibre orientation at printing start and end points

Fibre orientation varied at the start point and end point of the printing, as shown in Fig. 9. The start point of a straight line is the beginning of the extrusion. Polymer flow lagged behind nozzle movement, since extrusion pressure would have gradually built up in the nozzle after printing started until reaching a steady state of volumetric extrusion. Due to the narrower semi-drawn nature of the initial part of the extruded filament, fibres were highly oriented along the F direction, as expected based on the results in Fig. 4 for the narrower extrusion width. On the contrary, the end point of the printing showed low fibre orientation. Over-extrusion at the end of the line induced more lateral flow and out-of-plane flow, which is the natural direction of the material flowing out the nozzle as the nozzle stopped. Similarly, few fibres at the very tip at the start of extrusion (very left in the top part of the figure) were also less oriented than fibres in the rest of the filament.

Future research could consider the effects of pre-extrusion (un-retraction) at the beginning of the path and retraction at the end of the path. Retraction and un-retraction would significantly affect the extrudate geometry, but the results found here should still apply: fibres at the very tips (start and end) of the extruded filament will have greater Z orientation than the rest of the filament, and any narrower sections will have higher F-alignment of fibres than wider sections.

Die swell occurs for melt flow at nozzle exit [17]. It is hypothesised that fibre orientation decreases with increasing die swell ratios since it causes wider extrusion. Negative effects of die swell on fibre orientation was found via computational simulation [28] Since die swell ratios of non-Newtonian flow could be up to around 1.8 [18], future work could link die swell ratios to fibre orientation.

Melt flow rate and printing speed (nozzle velocity) are important factors related to rheology which could affect fibre orientation. Both increased printing speed and decreased flow rate lead to decreased W and H, where fibre orientation could change significantly [16]. Since the current research focuses on structural and geometric effects on fibre orientation, future study could explore how flow characteristics affects fibre orientation.

3.6. Case studies

This section extends the previous findings to more complicated structures and an alternative material. Two case studies consider realistic situations of 3D-printed objects including rectangular building
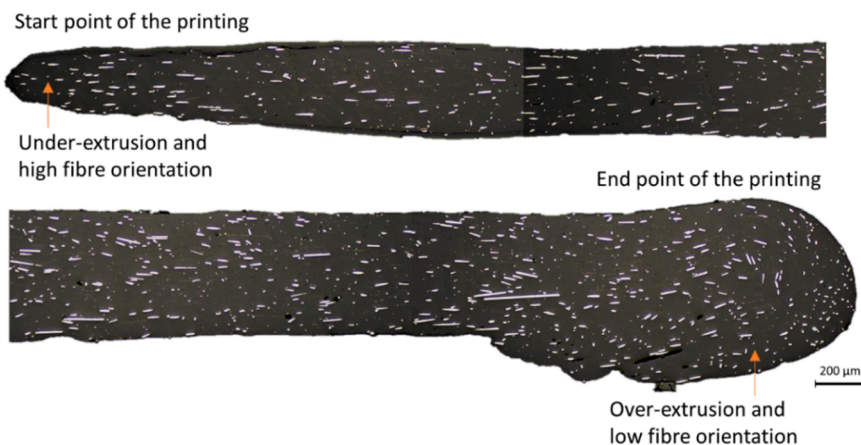

Fig. 9. Fibre orientation at start point and end point of the printing.

blocks and complicated shell-infill structure. Fibre orientation at corners and intersections for ABS-CF is compared to PLA-CF to test translatability of results.

3.6.1. Fibre orientation in 3D printed building blocks

Rectangular building blocks are common structure for solid regions in MEAM. A rectangular specimen with a length of 90 mm, width of 15 mm, and height of 3 mm was designed. It consisted of 15 layers, and all printed filaments were oriented unidirectionally in the F direction with W 0.6 mm and H 0.2 mm. The top-down views showed that fibres were highly oriented in the F direction, with F-alignment of 0.747, as shown in Fig. 10, which is similar to that found for single straight lines (0.748). For the cross-sections, the vast majority of fibres were oriented in the F-direction. However, there are a number of fibres oriented in the F-lateral-direction (a_{22} of 0.338), which is greater than single-filaments studied in Section 3.1, where fibres did not show much sideways lateral orientation with the same W and H. This might be caused by thermal diffusion when filaments are printed side-by-side. The extruded material likely flowed laterally from the nozzle than in single filaments since the neighbouring filament (printed on the previous pass of the nozzle) may have slightly blocked the newly deposited material, forcing it to move sideways from the nozzle. Compared to single-filament structures, multi-filament structures had slightly lower fibre orientation, but the overall trends were similar to those found for single extruded filaments.

3.6.2. Fibre orientation in a complicated shell-infill structure

A complicated print structure with a circular shell and infill structure was designed and 3D printed under the same printing conditions using PLA-CF. This 10-layer single-filament structure consisted of an outer circular shell of five concentric rings and internal lattice infill with multiple extrusion widths. The infill included three horizontal lines with W-0.4/0.6/0.8 mm in the figure (bottom-section), three vertical lines W-0.4/0.6/0.8 mm in the right-section, and four sinusoidal curves with W-0.6 mm and amplitude increasing by 2-fold, 4-fold and 6-fold, from left to right in the figure (left-section). The structure consists a broad range of conditions typical of a complicated print path generated in slicer software with different line widths, a range of intersections, solid perimeters and lattice-like internal structures, and a mixture of straight and curved lines as well as corners.

Micrographs of the specimen, including some with colour-coding based on in-plane fibre orientation, are shown in Fig. 11. Overall, fibres were highly aligned in the instantaneous F-direction of filaments: mostly red colour in the horizontal direction and mostly cyan colour in the vertical direction for straight lines. For the sinusoidal paths, consistent colour changes for every half period can be seen, which is consistent with the findings in Section 3.3. The fibre orientation in struts

with different W showed the same trend for F-alignment (W-0.4 > W-0.6 > W 0.8 mm) as found in the results Section 3.1.2. Fibre orientation decreased at both line-line intersections and line-curve intersections. The defected geometry (disrupted or wider/narrower extrusion before/after the intersection) found in the results section were also found. Overall, the findings in the main results section of this study clearly translated to this complicated print path. A framework of evaluating fibre orientation was built based on filament geometry and filament spatial relationships. By considering the print path as a collection of the universal structures identified and evaluated throughout this study, fibre orientation becomes scrutable and predictable. This case study demonstrates how the results of this study are of immediate value and potential benefit in terms of analysis of print path, setup of finite-element-analysis models, or print path generation and optimisation.

3.6.3. Finding translatability and validity

To test translatability to other materials, specimens for angular turns and intersections (cross and 'T' junction) were reproduced using ABS-CF with the same printer, same print paths, and reference W and H. For ABS, nozzle temperature was set to 240 °C, bed temperature was set to 90 °C and no cooling fan was used. ABS has considerably different chemical structures and properties to PLA (e.g. amorphous vs semi-crystalline, melting temperature range vs melting point, branched polymer chains vs linear chains, different melt viscosity), which make it appropriate to test translatability of the major findings. For the corners, similar trends of F-alignment, F-lat alignment, and Z-alignment with varied turning angles were found, as shown in Fig. 12 (a). This includes (1) a_{11} decreased from 30° to 90° and then increased to 150°; (2) a_{22} showed the opposite trend to a_{11} and peaked at 90°; and (3) a_{33} decreased from 30° to 150°. Additionally, a_{11} before, at, and after turns also showed the similar trend as PLA-CF, the data for which is included in Fig. S2. (a) in Supplementary Data. The average relative error of each data point with respect to PLA-CF was 16% for fibre orientation at corners, as shown in Fig. 12 (a), confirming high similarity between ABS-CF and PLA-CF. For the 'T' junction, ABS-CF always showed the same trend as PLA-CF before, at, and after junction for both first and second filament, as shown in Fig. 12 (b). The trends include (1) F-alignment recovery after junction for the first filament and (2) reduced F-alignment, increased F-lat alignment and increased Z-alignment at the junction for the second filament. That the same trends were found for PLA and ABS, even though they have considerably different viscoelastic and rheological properties [16], indicates that the results may translate to other polymers. However, specific alternative polymers should be investigated to confirm translatability, potentially by repeating the specimen-types most relevant to a particular study or application (e.g. widest/narrowest extrusion widths).
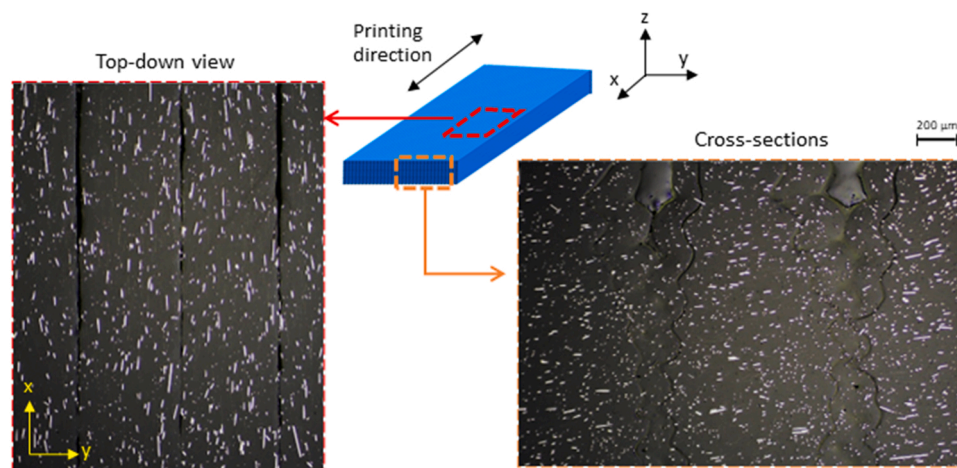

Fig. 10. Fibre orientation in building blocks of a rectangular specimen with micrographs of top-down view (x-y plane) and cross-sections (y-z plane).
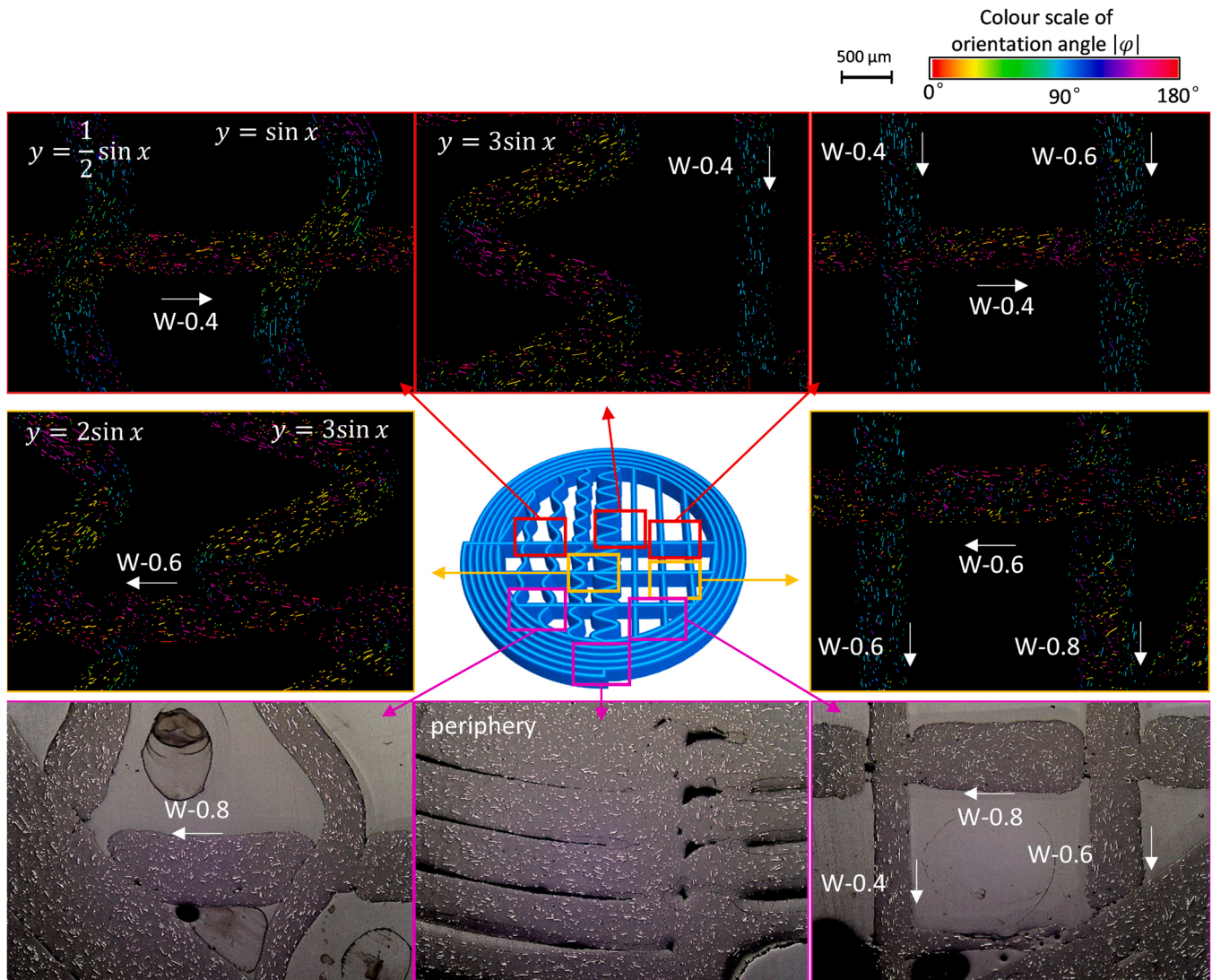
Fig. 11. Fibre orientation in a complicated print structure circular periphery and infill of straight lines and sinusoidal curves. Five micrographs on the top show fibre orientation. Fibres were coloured according to their in-plane orientation relative to horizontal in the figure (0 ° = direction to right). Three micrographs on the bottom show the printed structure and filament morphology without colour maps.

4. Conclusions

Fibre orientation in common fundamental 3D print structures and geometries was studied. Structures including straight paths, corners, a circular path, sinusoidal paths, and a range of intersections were parametrically designed and evaluated. Fibres were highly oriented in the instantaneous printing direction of each extruded filament, even in curved paths. By sectioning seven planes throughout thickness of a printed filament in the Z direction normal to the print-platform, variation in fibre orientation throughout the layer-thickness was found. For regions immediately below or above an interlayer bond, fibres were more oriented in the Z-oriented than for regions in the middle of the layer thickness. Increasing extrusion width and layer height led to a reduction in fibre alignment. Filament intersections and corners had lower fibre orientation than straight sections and inconsistent filament geometry, including narrow extrusion immediately after an intersection point between two extruded filaments on the same layer. Case studies of common building blocks and complex shell-infill structures demonstrated consistent fibre orientation in complicated structures with basic structures. Finally, ABS-CF showed similar trends of fibre orientation to PLA-CF, showing translatability of the main findings to different materials. The findings may be applied to control and predict short fibre

orientation for complicated structures. This study can significantly support future development of SCFRPs in terms of structural design, toolpath generation and simulation or evaluation of mechanics in fibre reinforced additive manufacturing.

CRediT authorship contribution statement

Jiongyi Yan: Writing – review & editing, Writing – original draft, Visualization, Validation, Software, Methodology, Investigation, Formal analysis, Data curation, Conceptualization. **Emrah Demirci:** Supervision, Resources. **Andrew Gleadall:** Writing – review & editing, Validation, Supervision, Resources, Project administration, Funding acquisition, Formal analysis, Data curation.

Declaration of Competing Interest

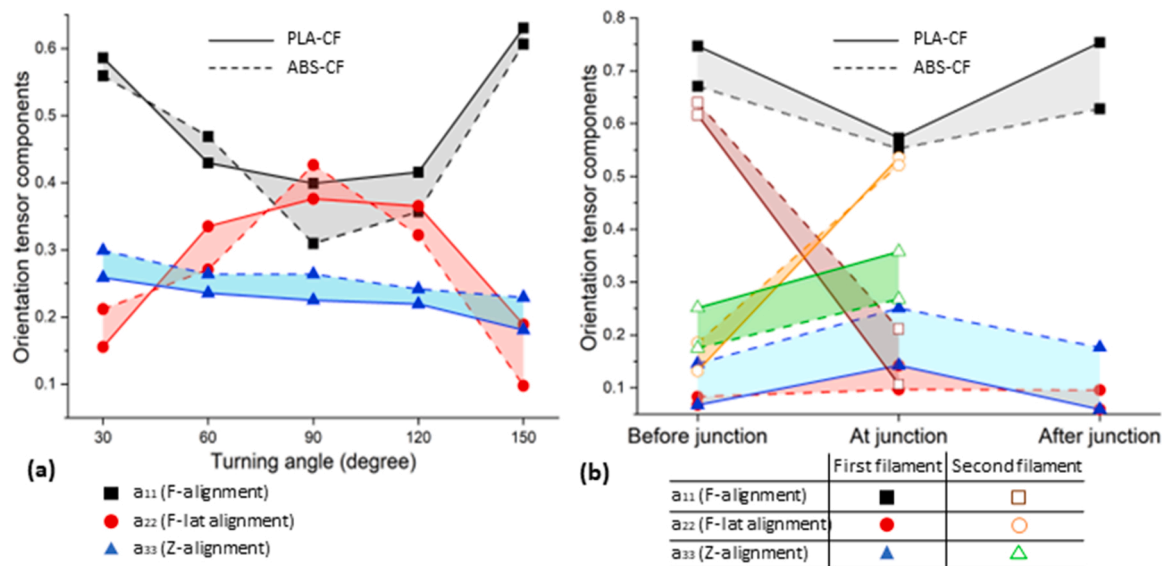The authors declare that they have no known competing financial

Fig. 12. Comparison of fibre orientation for PLA-CF and ABS-CF in different structures. (a) Fibre alignment at turns with different corner angles. (b) Fibre alignment at 'T' junction for both first and second filaments. Sharded areas indicate relative error of fibre orientation between two materials.

interests or personal relationships that could have appeared to influence the work reported in this paper.

Data Availability

Data will be made available on request.

Appendix A. Supporting information

Supplementary data associated with this article can be found in the online version at doi:10.1016/j.addma.2023.103535.

References

[1] N. Shahrubudin, T.C. Lee, R. Ramlan, An overview on 3D printing technology: technological, materials, and applications, Procedia Manuf. 35 (2019) 1286–1296, https://doi.org/10.1016/j.promfg.2019.06.089.

[2] A. Moumen, M. Tarfaoui, K. Lafdi, Additive manufacturing of polymer composites: processing and modeling approaches, Compos. Part B Eng. 171 (2019) 166–182, https://doi.org/10.1016/j.compositesb.2019.04.029.

[3] L.J. Love, V. Kunc, O. Rios, C.E. Duty, A.M. Elliott, B.K. Post, R.J. Smith, C.A. Blue, The importance of carbon fiber to polymer additive manufacturing, J. Mater. Res. 29 (2014) 1893–1898, https://doi.org/10.1557/jmr.2014.212.

[4] S. Wickramasinghe, T. Do, P. Tran, FDM-Based 3D printing of polymer and associated composite: a review on mechanical properties, defects and treatments, Polym. (Basel) 12 (2020) 1–42, https://doi.org/10.3390/polym12071529.

[5] B. Brenken, E. Barocio, A. Favaloro, V. Kunc, R.B. Pipes, Fused filament fabrication of fiber-reinforced polymers: a review, Addit. Manuf. 21 (2018) 1–16, https://doi.org/10.1016/j.addma.2018.01.002.

[6] T.Q. Tran, F.L. Ng, J.T.Y. Kai, S. Feih, M.L.S. Nai, Tensile strength enhancement of fused filament fabrication printed parts: a review of process improvement approaches and respective impact, Addit. Manuf. 54 (2022), 102724, https://doi.org/10.1016/j.addma.2022.102724.

[7] S.H.R. Sanei, D. Popescu, 3D-printed carbon fiber reinforced polymer composites: a systematic review, J. Compos. Sci. 4 (2020) 1–23, https://doi.org/10.3390/jcs4030098.

[8] G.D. Goh, Y.L. Yap, S. Agarwala, W.Y. Yeong, Recent progress in additive manufacturing of fiber reinforced polymer composite, Adv. Mater. Technol. 4 (2019) 1–22, https://doi.org/10.1002/admt.201800271.

[9] N. van de Werken, H. Tekinalp, P. Khanbolouki, S. Ozcan, A. Williams, M. Tehrani, Additively manufactured carbon fiber-reinforced composites: State of the art and perspective, Addit. Manuf. 31 (2020), 100962, https://doi.org/10.1016/j.addma.2019.100962.

[10] D. Zindani, K. Kumar, An insight into additive manufacturing of fiber reinforced polymer composite, Int. J. Light. Mater. Manuf. 2 (2019) 267–278, https://doi.org/10.1016/j.ijlmm.2019.08.004.

[11] V.R. Riley, J.L. Reddaway, Tensile strength and failure mechanics of fibre composites, J. Mater. Sci. 3 (1968) 41–46, https://doi.org/10.1007/BF00550888.

[12] R. Byron Pipes, R.L. McCullough, D.G. Taggart, Behavior of discontinuous fiber composites: fiber orientation, Polym. Compos. 3 (1982) 34–39, https://doi.org/10.1002/pc.750030107.

[13] Z.M. Huang, L.M. Xin, Stress concentration factors of matrix in composite under transverse loads, 2015-July, ICCM Int. Conf. Compos. Mater. (2015) 19–24.

[14] J. Yan, E. Demirci, A. Ganesan, A. Gleadall, Extrusion width critically affects fibre orientation in short fibre reinforced material extrusion additive manufacturing, Addit. Manuf. 49 (2022), 102496, https://doi.org/10.1016/j.addma.2021.102496.

[15] Z. Wang, D.E. Smith, A fully coupled simulation of planar deposition flow and fiber orientation in polymer composites additive manufacturing, Materials 14 (2021) 1–27, https://doi.org/10.3390/ma14102596.

[16] J.F. Agassant, F. Pigeonneau, L. Sardo, M. Vincent, Flow analysis of the polymer spreading during extrusion additive manufacturing, Addit. Manuf. 29 (2019), 100794, https://doi.org/10.1016/j.addma.2019.100794.

[17] B.P. Heller, D.E. Smith, D.A. Jack, Effects of extrudate swell and nozzle geometry on fiber orientation in Fused Filament Fabrication nozzle flow, Addit. Manuf. 12 (2016) 252–264, https://doi.org/10.1016/j.addma.2016.06.005.

[18] T. Van Waeleghem, F.H. Marchesini, L. Cardon, D.R. D'hooge, Melt exit flow modelling and experimental validation for fused filament fabrication: from Newtonian to non-Newtonian effects, J. Manuf. Process 77 (2022) 138–150, https://doi.org/10.1016/j.jmapro.2022.03.002.

[19] H.L. Tekinalp, V. Kunc, G.M. Velez-Garcia, C.E. Duty, L.J. Love, A.K. Naskar, C. A. Blue, S. Ozcan, Highly oriented carbon fiber-polymer composites via additive manufacturing, Compos. Sci. Technol. 105 (2014) 144–150, https://doi.org/10.1016/j.compscitech.2014.10.009.

[20] R.S. Bay, Stereological measurement and error estimates for three-dimensional fiber orientation, Polym. Eng. Sci. 32 (1992) 240–253.

[21] R.S. Chisena, S.M. Engstrom, A.J. Shih, Computed tomography evaluation of the porosity and fiber orientation in a short carbon fiber material extrusion filament and part, Addit. Manuf. 34 (2020), https://doi.org/10.1016/j.addma.2020.101189.

[22] D. Yang, H. Zhang, J. Wu, E.D. McCarthy, Fibre flow and void formation in 3D printing of short-fibre reinforced thermoplastic composites: An experimental benchmark exercise, Addit. Manuf. 37 (2021), 101686, https://doi.org/10.1016/j.addma.2020.101686.

[23] M. Spoerk, C. Savandaiah, F. Arbeiter, G. Traxler, L. Cardon, C. Holzer, J. Sapkota, Anisotropic properties of oriented short carbon fibre filled polypropylene parts fabricated by extrusion-based additive manufacturing, Compos. Part A Appl. Sci. Manuf. 113 (2018) 95–104, https://doi.org/10.1016/j.compositesa.2018.06.018.

[24] W. Zhang, C. Cotton, J. Sun, D. Heider, B. Gu, B. Sun, T.W. Chou, Interfacial bonding strength of short carbon fiber/acrylonitrile-butadiene-styrene composites fabricated by fused deposition modeling, Compos. Part B Eng. 137 (2018) 51–59, https://doi.org/10.1016/j.compositesb.2017.11.018.

[25] R.T.L. Ferreira, I.C. Amatte, T.A. Dutra, D. Bürger, Experimental characterization and micrography of 3D printed PLA and PLA reinforced with short carbon fibers, Compos. Part B Eng. 124 (2017) 88–100, https://doi.org/10.1016/j.compositesb.2017.05.013.

[26] E.A. Papon, A. Haque, Fracture toughness of additively manufactured carbon fiber reinforced composites, Addit. Manuf. 26 (2019) 41–52, https://doi.org/10.1016/j.addma.2018.12.010.

[27] M. Ivey, G.W. Melenka, J.P. Carey, C. Ayranci, Characterizing short-fiber-reinforced composites produced using additive manufacturing, Adv. Manuf. Polym. Compos. Sci. 3 (2017) 81–91, https://doi.org/10.1080/20550340.2017.1341125.

[28] B.P. Heller, D.E. Smith, D.A. Jack, Planar deposition flow modeling of fiber filled composites in large area additive manufacturing, Addit. Manuf. 25 (2019) 227–238, https://doi.org/10.1016/j.addma.2018.10.031.

[29] Z. Wang, D.E. Smith, The Effect of Polymer Melt Rheology on Predicted Die Swell and Fiber Orientation in Fused Filament Fabrication Nozzle Flow, in: Solid Free. Fabr. Symp., 2017, pp. 1082–1095. ⟨http://sffsymposium.engr.utexas.edu/sites/default/files/2017/Manuscripts/TheEffectofPolymerMeltRheologyonPredictedD.pdf⟩.

[30] Z. Wang, D.E. Smith, Finite element modelling of fully-coupled flow/fiber-orientation effects in polymer composite deposition additive manufacturing nozzle-extrudate flow, Compos. Part B Eng. 219 (2021), 108811, https://doi.org/10.1016/j.compositesb.2021.108811.

[31] D. Yang, K. Wu, L. Wan, Y. Sheng, A particle element approach for modelling the 3D printing process of fibre reinforced polymer composites, J. Manuf. Mater. Process 1 (2017) 1–11, https://doi.org/10.3390/jmmp1010010.

[32] G.D.L. Goh, Y.L. Yap, H.K.J. Tan, S.L. Sing, G.D.L. Goh, W.Y. Yeong, Process–structure–properties in polymer additive manufacturing via material extrusion: a review, Crit. Rev. Solid State Mater. Sci. 45 (2020) 113–133, https://doi.org/10.1080/10408436.2018.1549977.

[33] P. Pibulchinda, E. Barocio, R.B. Pipes, Influence of fiber orientation on deformation of additive manufactured composites, Addit. Manuf. 49 (2022), 102483, https://doi.org/10.1016/j.addma.2021.102483.

[34] J. Kim, B.S. Kang, Enhancing structural performance of short fiber reinforced objects through customized tool-path, Appl. Sci. 10 (2020) 1–19, https://doi.org/10.3390/app10228168.

[35] G. Andy, FullControl GCODE Designer: open source software for unconstrained design in additive manufacturing. Submitted for publication. Software available at: ⟨www.fullcontrolgcode.com⟩., (2019).

[36] G. Percoco, L. Arleo, G. Stano, F. Bottiglione, Analytical model to predict the extrusion force as a function of the layer height, in extrusion based 3D printing, Addit. Manuf. 38 (2021), 101791, https://doi.org/10.1016/j.addma.2020.101791.

[37] J. Yan, E. Demirci, A. Gleadall, Material-independent mechanical anisotropy and fracture mechanisms in fibre reinforced material extrusion additive manufacturing, Http//Dx.Doi.Org/10.2139/Ssrn.4074214. (n.d.).

[38] T. Mollah, A. Moetazedian, A. Gleadall, J. Yan, W.E. Alphonso, R. Comminal, B. Seta, T. Lock, J. Spangenberg, Investigation on corner precision at different corner angles in material extrusion additive manufacturing: An experimental and computational fluid dynamics analysis, in: Solid Free. Fabr. 2022 Proc. 33rd Annu. Int. Solid Free. Fabr. Symp. Univ. Texas Austin, 2022: pp. 872–881.